ELSEVIER

Journal of Wind Engineering
and Industrial Aerodynamics 67&68 (1997) 183–193

JOURNAL OF
wind engineering
AND
industrial
aerodynamics

Two dimensional discrete vortex method for application to bluff body aerodynamics

Jens Honoré Walther[a,*], Allan Larsen[b]

[a] *Danish Maritime Institute, Hjortekærsvej 99, DK-2800 Lyngby, Denmark*
[b] *COWI A/S, Parallelvej 15, DK-2800 Lyngby, Denmark*

Abstract

Two-dimensional viscous incompressible flow past a flat plate of finite thickness and length is simulated using the discrete vortex method. Both a fixed plate and a plate undergoing a harmonic heave and pitch motion are studied. The Reynolds number is 10^4 and the reduced onset flow speed, U/fc is in the range 2–14. The fundamental kinematic relation between the velocity and the vorticity is used in a novel approach to determine the surface vorticity. An efficient influence matrix technique is used in a fast adaptive multipole algorithm context to obtain a mesh-free method. The numerical results are compared with the steady-state Blasius solution, and with the inviscid solution for the flow past an oscillating plate by Theodorsen.

Keywords: Discrete vortex method; Vorticity boundary condition; Conservation of vorticity moments; Flow past a flat plate; Aerodynamic derivatives

1. Introduction

The flow past a flat plate, both fixed and in heave or pitch motion serves as a realistic but simple test case for the numerical study of flow past oscillating bluff bodies. The flow possesses most of the features of bluff body flows, e.g., boundary-layer growth, vortex shedding and interaction between free shear layers. Also the results can be compared with the steady-state solution due to Blasius regarding the boundary-layer characteristics, cf. Ref. [1], and with the inviscid solution by Theodorsen for the oscillating plate [2]. For small amplitudes and relatively high Reynolds numbers the discrete vortex method results are expected to compare well with the inviscid results.

* Corresponding author. E-mail: jhw@danishmaritime.dk.

PII S0167-6105(97)00072-X

In an accompanying paper [3], extensive tests are presented using the present method for aeroelastic analysis of bridge sections.

2. Mathematical formulation

2.1. Kinetic and kinematic relations

The kinetics of a two-dimensional laminar flow with constant kinematic viscosity ν and density ρ in a domain $\mathscr{D}$ bounded by $\partial\mathscr{D} = \mathscr{B}$ is governed by the vorticity transport equation

$$\partial_t \omega + (\boldsymbol{v} \cdot \nabla)\omega = \nu \nabla^2 \omega \,, \tag{1}$$

where $\boldsymbol{v}(\boldsymbol{x}, t)$ is the velocity and $\boldsymbol{\omega}(\boldsymbol{x}, t) = \omega(\boldsymbol{x}, t)\boldsymbol{e}_z$ the vorticity.

The kinematic relation between the velocity and the vorticity may be formulated as an integral equation, cf. [4]

$$\boldsymbol{v}(\boldsymbol{x}, t) = \boldsymbol{U}(t) - \frac{1}{2\pi} \int\int_{\mathscr{D}} \frac{\boldsymbol{\omega}_0 \times (\boldsymbol{x}_0 - \boldsymbol{x})}{|\boldsymbol{x}_0 - \boldsymbol{x}|^2} \, \mathrm{d}\mathscr{D}_0$$

$$+ \frac{1}{2\pi} \oint_{\mathscr{B}} \frac{(\boldsymbol{v}_0 \cdot \boldsymbol{n}_0)(\boldsymbol{x}_0 - \boldsymbol{x}) - (\boldsymbol{v}_0 \times \boldsymbol{n}_0) \times (\boldsymbol{x}_0 - \boldsymbol{x})}{|\boldsymbol{x}_0 - \boldsymbol{x}|^2} \, \mathrm{d}\mathscr{B}_0 \,, \tag{2}$$

where $\boldsymbol{U}(t)$ is the irrotational onset flow, $\boldsymbol{n}$ is the surface normal, and $\boldsymbol{v}$ is the velocity at the surface. The boundary integral accounts for the vorticity not included in $\mathscr{D}$. Hence, if $\mathscr{D}$ contains all non-zero vorticity, the contribution from the surface integral vanishes.

2.2. Vorticity boundary conditions

Following the work of Wu and Gulcat [5], the value of the vorticity at the solid boundary is found via the kinematic relation (2), where the value of both the volume and surface integrals are known, except the contribution from the surface vorticity, i.e.,

$$\int\int_{\mathscr{D}_\mathscr{B}} \frac{\boldsymbol{\omega}_0 (\boldsymbol{x}_0 - \boldsymbol{x}_\mathscr{B})}{|\boldsymbol{x}_0 - \boldsymbol{x}_\mathscr{B}|^2} \, \mathrm{d}\mathscr{D}_0 = \mathscr{T}(\boldsymbol{x}_\mathscr{B}) + 2\pi[\boldsymbol{U}(t) - \boldsymbol{v}(\boldsymbol{x}_\mathscr{B})] \,, \tag{3}$$

where $\mathscr{D}_\mathscr{B}$ is a "thin" layer adjacent to the surface $\mathscr{B}$, and the vector $\mathscr{T}(\boldsymbol{x}_\mathscr{B})$ is the induced velocity from the vorticity in the fluid and solids excluding the surface

vorticity

$$\mathscr{T}(\boldsymbol{x}_{\mathscr{B}}) = \oint_{\mathscr{B}} \frac{(\boldsymbol{v}_0 \cdot \boldsymbol{n}_0)(\boldsymbol{x}_0 - \boldsymbol{x}_{\mathscr{B}}) - (\boldsymbol{v}_0 \times \boldsymbol{n}_0) \times (\boldsymbol{x}_0 - \boldsymbol{x}_{\mathscr{B}})}{|\boldsymbol{x}_0 - \boldsymbol{x}_{\mathscr{B}}|^2} \, \mathrm{d}\mathscr{B}_0$$

$$- \int_{\mathscr{S}-\mathscr{S}_{\mathscr{B}}} \int \frac{\boldsymbol{\omega}_0 \times (\boldsymbol{x}_0 - \boldsymbol{x}_{\mathscr{B}})}{|\boldsymbol{x}_0 - \boldsymbol{x}_{\mathscr{B}}|^2} \, \mathrm{d}\mathscr{D}_0 \,. \tag{4}$$

In the vortex method context it is convenient to introduce the surface vortex sheet, γ

$$\frac{\partial \gamma}{\partial n} = \omega \,, \tag{5}$$

where n is the surface normal, thus, using Eq. (5) in (4) gives

$$\int_{\mathscr{B}} \frac{\gamma_0 \boldsymbol{e}_z \times (\boldsymbol{x}_0 - \boldsymbol{x}_{\mathscr{B}})}{|\boldsymbol{x}_0 - \boldsymbol{x}_{\mathscr{B}}|^2} \, \mathrm{d}\mathscr{B}_0 = \mathscr{T}(\boldsymbol{x}_{\mathscr{B}}) + 2\pi[\boldsymbol{U}(t) - \boldsymbol{v}(\boldsymbol{x}_{\mathscr{B}})]. \tag{6}$$

The components of the vector equation (6) are Fredholm integral equations in the unknown γ_0. The solution is unique up to a constant, i.e. an infinite number of solutions exist, cf. Ref. [4]. The solution is made unique by imposing the global constraint on the vorticity, that the time rate of change of the total vorticity in both the solid ($\mathscr{S}$) and fluid domain ($\mathscr{F}$) is zero

$$\partial t \int_{\mathscr{F} \cup \mathscr{S}} \int \omega \, \mathrm{d}\mathscr{D} = 0. \tag{7}$$

Moreover, if the total vorticity is zero at $t = 0$ it remains zero for $t > 0$. Thus for each solid, Eq. (7) is imposed making the system of equations overdetermined. Eqs. (6) and (7) are solved in the least-squares sense.

In the previous implementations, e.g. Refs. [4, 6–9] Eq. (6) is solved for zero tangential velocity. In the present study Eq. (6) is solved for the normal component. Thus, the no-slip condition is imposed implicitly as a consequence of Eqs. (6) and (7).

3. Vortex method

The Lagrangian solution to Eqs. (1) and (2) involves tracking individual fluid elements ($\boldsymbol{x}_p$, Γ_p) according to

$$\frac{\mathrm{d}\boldsymbol{x}_p}{\mathrm{d}t} = \boldsymbol{v}(\boldsymbol{x}_p, t) \,, \tag{8}$$

$$\frac{\mathrm{d}\omega}{\mathrm{d}t} = \nu \nabla^2 \omega \,, \tag{9}$$

where $\boldsymbol{v}(\boldsymbol{x}_p, t)$ is approximated from Eq. (2)

$$\boldsymbol{v}(\boldsymbol{x}_p, t) = \boldsymbol{U}(t) - \frac{1}{2\pi}\sum_{j=1}^{n_s}\oint_{\mathscr{B}_j}\frac{(\gamma_0\boldsymbol{e}_z + \boldsymbol{v}_0\times\boldsymbol{n}_0)\times(\boldsymbol{x}_0-\boldsymbol{x}_p) - (\boldsymbol{v}_0\cdot\boldsymbol{n}_0)(\boldsymbol{x}_0-\boldsymbol{x}_p)}{|\boldsymbol{x}_0-\boldsymbol{x}_p|^2}\,\mathrm{d}\mathscr{B}_0 - \frac{1}{2\pi}\sum_{i=1}^{n_v}\frac{\Gamma_i\boldsymbol{e}_z\times(\boldsymbol{x}_i-\boldsymbol{x}_p)}{|\boldsymbol{x}_i-\boldsymbol{x}_p|^2}. \tag{10}$$

n_s is the number of solids, and n_v is the number of free vortices with vortex strength, Γ_i. The singular vortex–vortex interaction in Eq. (10) is regularised by applying a Gaussian core function. The solids are approximated by polygons and the surface vortex sheet and surface velocity are given a linear variation when evaluating Eq. (10), and when solving Eq. (6).

Eq. (8) is solved numerically by standard ordinary differential equation methods. The diffusion equation (9) is approximated by random walks, thus, the solution to Eqs. (8) and (9) using Euler integration is

$$\boldsymbol{x}_p^{k+1} = \boldsymbol{x}_p^k + \boldsymbol{v}(\boldsymbol{x}_p^k)\Delta t + \boldsymbol{\eta}_p, \tag{11}$$

where $\boldsymbol{x}_p^k$ is the position of the fluid element at the kth time step, Δt is the time step, and $\boldsymbol{\eta}_p$ are random numbers with zero mean and variance $2\nu\Delta t$.

The surface vortex sheets are converted into vortex blobs and, subsequently, diffused into the flow by one-sided random walks. Vortices already in the flow entering the solids by a random walk are removed from the calculations. The conservation of the total vorticity (7) is modified accordingly,

$$\sum_{i=1}^{m_j}\frac{\gamma_{ij}^k - \gamma_{ij}^{a,k-1}}{\Delta t}\Delta s_{ij} + 2A_j\frac{\Omega_j^k - \Omega_j^{k-1}}{\Delta t} = 0, \tag{12}$$

for each jth solid. m_j is the number of boundary elements, γ_{ij}^k is the released circulation at the kth time step, $\gamma_{ij}^{a,k-1}$ is the annihilated circulation from the previous time step, Ω_j is the angular velocity, and A_j is the area of the solid.

The costly $\mathcal{O}(n_v^2)$ operations imposed by the kinematic relation (2) are overcome by the $\mathcal{O}(n_v)$ fast adaptive multipole algorithm in Ref. [10], see also Ref. [11] for details regarding the implementation. Also, to limit the number of computational elements, vortices in the wake are amalgamated when sufficiently far downstream the solid bodies, here $|\boldsymbol{x}_p| > 6$. Two vortices are merged to satisfy the zeroth and first-order vorticity moment, provided they satisfy the following expression:

$$\left|\frac{\Gamma_i\Gamma_j}{\Gamma_i+\Gamma_j}\right||\boldsymbol{x}_i-\boldsymbol{x}_j| < \varepsilon, \tag{13}$$

where ε is a small number, cf. Ref. [12].

3.1. Aerodynamic forces

The aerodynamic forces are found by a momentum balance, or by integrating the surface pressure. The derivations are given in Refs. [11,13].

3.1.1. Momentum balance

Considering a momentum balance, the total aerodynamic forces are given by

$$\boldsymbol{F} = -\rho \frac{\mathrm{d}\boldsymbol{\alpha}}{\mathrm{d}t} + \rho \sum_{j=1}^{n_s} \frac{\mathrm{d}}{\mathrm{d}t} \int\int_{\mathscr{S}_j} \boldsymbol{v}\, \mathrm{d}\mathscr{D}\,, \tag{14}$$

where $\boldsymbol{\alpha}$ is the first-order moment of the vorticity

$$\boldsymbol{\alpha} = \int\int_{\mathscr{D}} \boldsymbol{x} \times \boldsymbol{\omega}\, \mathrm{d}\mathscr{D}\,. \tag{15}$$

For a general translating and rotating body (described by the position of the centre of rotation, $\boldsymbol{x}_{\mathrm{rot}}$ and the angle of attack, θ) it is easy to show that Eq. (14) can be written as

$$F = -\rho\left(\frac{\mathrm{d}\boldsymbol{\alpha}}{\mathrm{d}t}\right)_{\mathscr{F}} + \rho \frac{\mathrm{d}}{\mathrm{d}t} \sum_{j=1}^{n_s} \left[\boldsymbol{v}_{\mathrm{rot}} A_j + 2\Omega_j A_j \boldsymbol{e}_z \times \boldsymbol{x}_{\mathrm{rot}} + 3\Omega_j \boldsymbol{e}_z \times \boldsymbol{M}_j\right], \tag{16}$$

where $\boldsymbol{v}_{\mathrm{rot}}$ is the velocity of the centre of rotation, and $\boldsymbol{M}_j$ is the first-order moment of area of the jth solid

$$\boldsymbol{M}_j = \int\int_{\mathscr{S}_j} (\boldsymbol{x} - \boldsymbol{x}_{\mathrm{rot}})\, \mathrm{d}\mathscr{D}\,. \tag{17}$$

The first-order moment of the vorticity is approximated by the sum

$$\boldsymbol{\alpha} \approx \sum_{i=1}^{n_v} \boldsymbol{x}_i \times \boldsymbol{e}_z \Gamma_i\,. \tag{18}$$

3.1.2. Surface pressure

From the integral expression (14) the forces on the individual solid bodies, not given its nature, the local loads can be determined. To this end, the local pressure distribution is needed.

Given the no-slip boundary condition, the Naviér–Stokes equations reduce to

$$\frac{1}{\rho}\frac{\partial p}{\partial s} = -\nu \frac{\partial \omega}{\partial n} - a_s\,, \tag{19}$$

where n and s are the normal and tangential direction, and a_s is the tangential acceleration of the boundary. Now neglecting the streamwise diffusion at the solid

boundary, the vorticity transport equation (1) reads

$$\frac{\partial \omega}{\partial t} = \nu \frac{\partial^2 \omega}{\partial n^2}, \tag{20}$$

and using Eq. (5) gives

$$\frac{\partial \gamma}{\partial t} = \nu \frac{\partial \omega}{\partial n}. \tag{21}$$

Inserting Eq. (21) in Eq. (19) gives

$$\frac{1}{\rho}\frac{\partial p}{\partial s} = -\frac{\partial \gamma}{\partial t} - a_s. \tag{22}$$

The flux of circulation, $(\partial\gamma/\partial t)$ at the ith boundary element of the jth solid is given by

$$\left(\frac{\partial \gamma}{\partial t}\right)_{ij} \approx \frac{\gamma_{ij}^{k} - \gamma_{ij}^{a,k-1}}{\Delta t}. \tag{23}$$

Thus Eq. (22) is integrated using Eq. (23) along the solid boundary to compute the pressure distribution. Notice that by virtue of Eq. (12) the pressure is singled-valued since

$$\frac{1}{\rho}\oint_{\mathscr{B}_j} \frac{\partial p}{\partial s}\,\mathrm{d}\mathscr{B} = -\oint_{\mathscr{B}_j} \frac{\partial \gamma}{\partial t}\,\mathrm{d}\mathscr{B} - \frac{\partial}{\partial t}\oint_{\mathscr{B}_j} v_s\,\mathrm{d}\mathscr{B} \tag{24}$$

$$= -\oint_{\mathscr{B}_j} \frac{\partial \gamma}{\partial t}\,\mathrm{d}\mathscr{B} - \frac{\partial}{\partial t}\int\int_{\mathscr{D}_j} \boldsymbol{\omega}\cdot\boldsymbol{e}_z\,\mathrm{d}\mathscr{D} \tag{25}$$

$$\approx -\sum_{i=1}^{m_j} \frac{\gamma_{ij}^{k} - \gamma_{ij}^{a,k-1}}{\Delta t}\Delta s_{ij} - 2A_{ij}\frac{\Omega_j^{k} - \Omega_j^{k-1}}{\Delta t} = 0. \tag{26}$$

4. Simulation of unsteady flow past a flat plate

4.1. Fixed plate

The flow past a fixed flat plate at Reynolds number 10^4 is simulated to confirm the ability of the present method to accurately predict boundary-layer growth, and to validate the implicit enforcement of the no-slip condition. The plate is given a finite thickness (H) to obtain a non-trivial potential flow at $t = 0^+$ (the potential flow past an infinite thin plate is $\gamma_i = 0, \forall i$). The necessary thickness of the plate to prevent vortices "diffusing" across the plate is restricted by the Reynolds number and the time-step size, or equivalently, the standard deviation of the random walk, hence $H > 3\sqrt{2\nu\Delta t}$. The chord length (c) and onset flow speed (U) are unity, and a chord-to-thickness ratio of 200 is used throughout. Approximately 400 boundary elements

are used to discretize the plate. The vortices are advanced in time using the second-order Adams–Bashforth scheme with a time step of 0.005.

Velocity profiles are computed at 40 x coordinate positions equidistantly spaced along the plate, each profile consisting of 20 velocities. The simulation is carried out to $t = 6$, sampling the velocity profiles from $t = 5$ to 6, with a total of 20 samples.

Fig. 1 shows the position of the vortices close to the plate at time $t = 6$. A boundary layer is clearly visible, and the wake extending six chord lengths downstream (not shown) is unstable showing Kelvin–Helmholtz instability.

The time-average boundary-layer thickness (δ), displacement thickness (δ_1), and momentum thickness (δ_2) are displayed in Fig. 2. An excellent agreement is observed for $x/c < 0.8$. The predicted shape factor is $H_{12} = \delta_1/\delta_2 = 2.5$, -4% off the Blasius value of 2.6. Fig. 3 shows the 10 centre velocity profiles ($0.38 > x/c > 0.68$). Again an excellent agreement is observed, and the no-slip condition is reasonably satisfied.

For lower Reynolds numbers (not presented), the presence of the trailing edge is felt for smaller x co-ordinate values ($x/c < 0.5$). At higher Reynolds numbers the

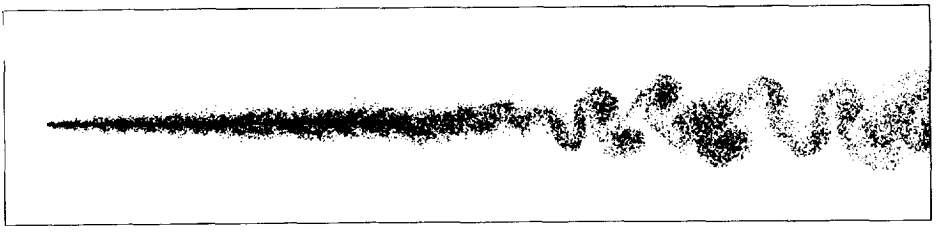

Fig. 1. Position of the vortices for the flow past a fixed flat plate at Reynolds number 10^4. The wake extends approximately six chord lengths downstream (not shown).

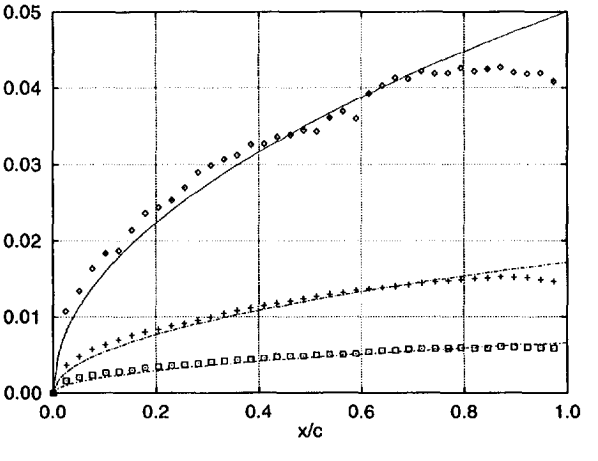

Fig. 2. Time-average boundary-layer characteristics for the viscous flow past a fixed flat plate at Reynolds number 10^4. The profiles are based on 20 velocity samples from $t = 5$–6. Theory: (———) Blasius; present results: (◇) boundary-layer thickness; (+) displacement thickness; (□) momentum thickness.

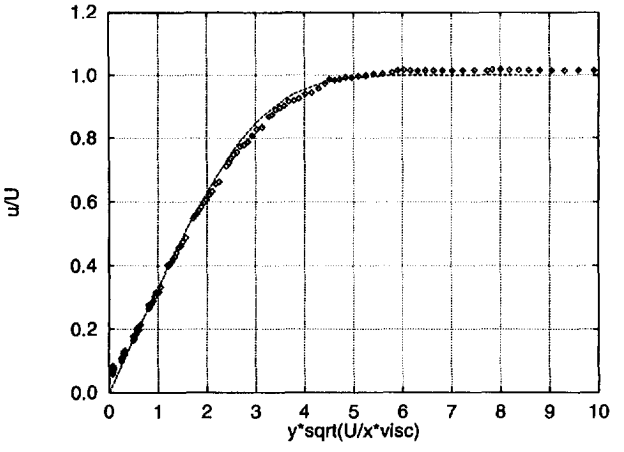

Fig. 3. Time-averaged velocity distribution in the boundary-layer of a fixed flat plate at Reynolds number 10^4. Theory (———), Blasius solution; (◇) present results.

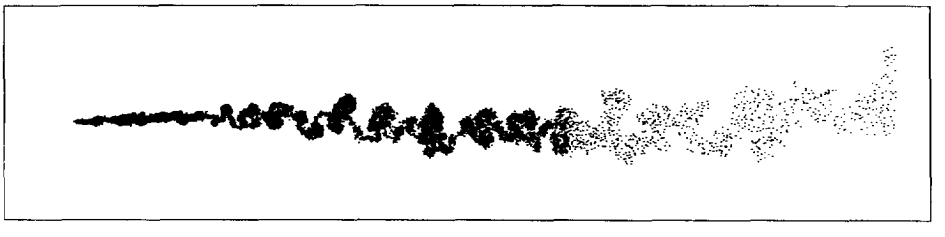

Fig. 4. Position of the vortices for the flow past a flat plate at Reynolds number 10^4 undergoing a harmonic pitch motion. The wake extends approximately 32 chord lengths downstream (not shown). $v_r = 12$ and $t = 32$.

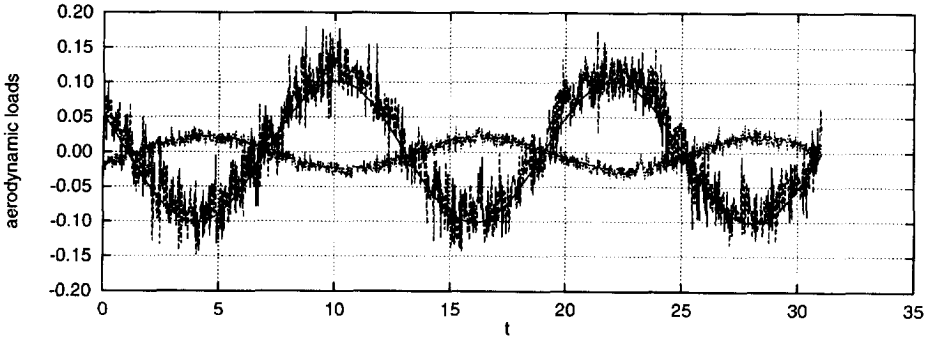

Fig. 5. Time history of the aerodynamic lift and moment for the flow past a flat plate in pitch motion at Reynolds number 10^4. $v_r = 12$. Vortex method: (— —) lift; (– – –) moment. Modelled lift and moment from Eqs. (27) and (28) (—).

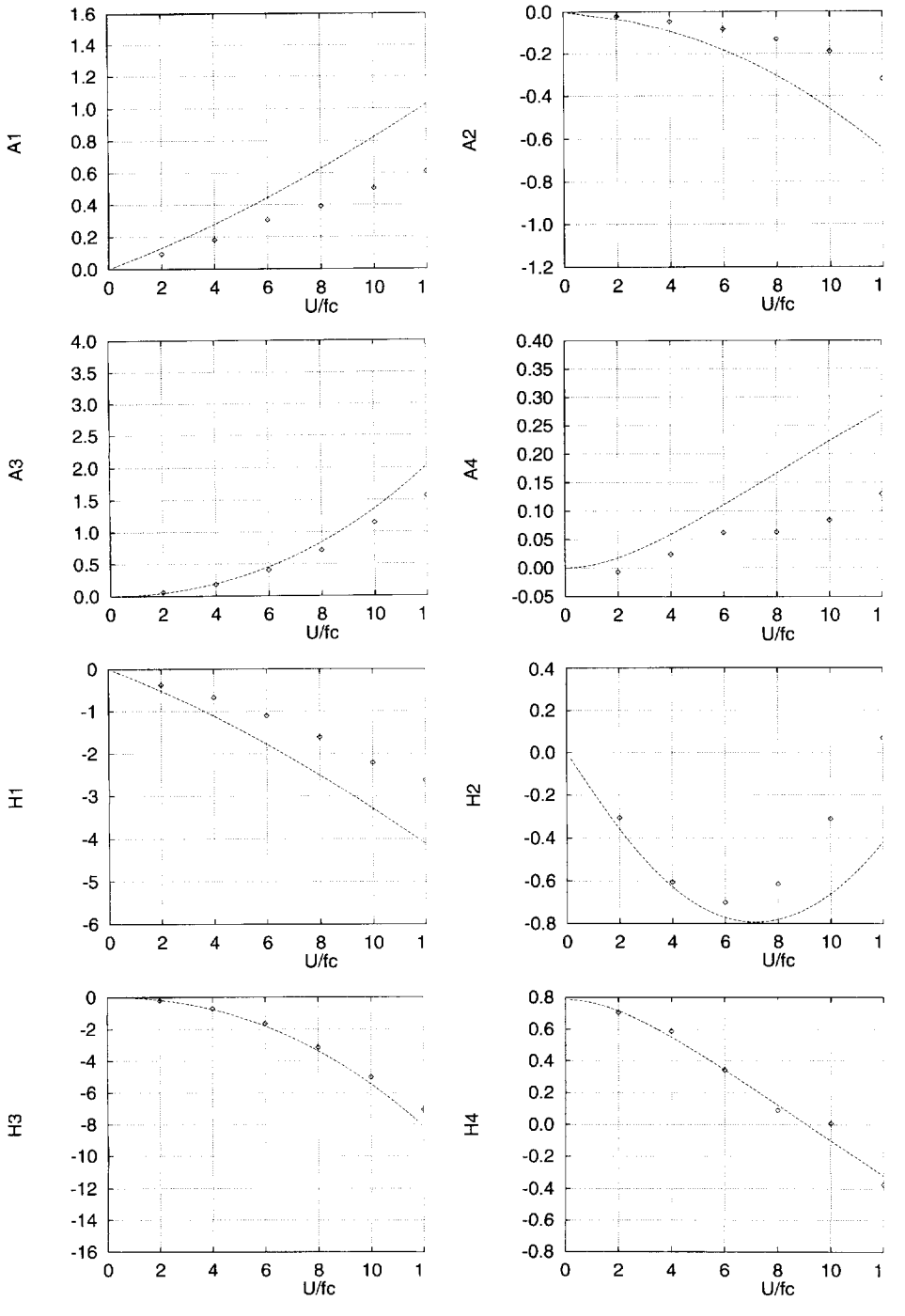

Fig. 6. Aerodynamic derivatives for the flow past a flat plate at Reynolds number 10^4. (◇) present results; (—) inviscid theory [2].

boundary-layer is no longer stable showing large coherent structures travelling downstream with a speed of approximately 0.5 U, cf. Ref. [11].

4.2. Oscillating plate

The flow past a flat plate undergoing a harmonic heave ($h(t) = A_h \sin(2\pi ft)$) or pitch motion ($\theta(t) = A_\theta \sin(2\pi ft)$) depends on the Reynolds number, the reduced onset flow speed, $v_r = U/(fc)$, and the amplitude and the centre of the oscillation.

Using 200 boundary elements the plate is oscillated in heave and pitch about the half-chord with an amplitude of $A_h = 0.02$–0.05, and $A_\theta = 3$–5°, respectively. The time step is 0.025 and the vortices are advanced using the Euler scheme.

Fig. 4 shows the position of the vortices for the flow past a flat plate in pitch motion at $t = 32$ and $v_r = 12$. Notice, the vortex amalgamation for $x/c > 6$. Fig. 5 shows the corresponding aerodynamic lift and moment and the modelled loads as given by the aerodynamic derivatives

$$L = \frac{1}{2}\rho U^2 2c\left[KH_1^*\frac{\dot{h}}{U} + KH_2^*\frac{c\dot{\theta}}{U} + K^2H_3^*\theta + K^2H_4^*\frac{h}{c}\right], \tag{27}$$

$$M = \frac{1}{2}\rho U^2 2c^2\left[KA_1^*\frac{\dot{h}}{U} + KA_2^*\frac{c\dot{\theta}}{U} + K^2A_3^*\theta + K^2A_4^*\frac{h}{c}\right], \tag{28}$$

where $K = 2\pi fc/U$ is the reduced frequency, and L and M are the aerodynamic lift and moment, cf. Ref. [14]. Fig. 6 compares the extracted aerodynamic derivatives with the inviscid derivatives in Ref. [2]. The damping coefficients, H_1^*, H_2^*, A_1^*, and A_2^* are, in general, underpredicted as should be expected. The stiffness coefficients are, in general, are in good agreement with the inviscid results, in particular, the lift and moment slope (H_3^*, and A_3^*) are in excellent agreement with the theoretical values.

5. Conclusions

In the present study, the flow past a flat plate is simulated using a mesh-free discrete vortex method. A novel vorticity boundary condition is introduced based on the fundamental kinematic relation between the velocity and the vorticity. The surface vorticity is found using an efficient boundary element method which imposes the no-penetration velocity boundary condition, and the conservation of the total vorticity. Hence, the no-slip condition is enforced implicity. The costly evaluation of the kinematic relation is efficiently handled by the $\mathcal{O}(n_v)$ adaptive multipole expansion algorithm.

The flow past a fixed and harmonically oscillating flat plate is used as a generic flow past oscillating bluff bodies. The predicted boundary-layer characteristics are in excellent agreement with the steady-state Blasius flow, and the extracted aerodynamic derivatives are in good to excellent agreement with the theoretical inviscid derivatives by Theodorsen.

Acknowledgements

This work was financially supported by the COWI foundation.

References

[1] H. Schlichting, Boundary-Layer Theory, 7th ed., McGraw-Hill, New York, 1979.
[2] T. Theodorsen, General theory of aerodynamic instability and the mechanism of flutter, TR 496, NACA, 1935.
[3] A. Larsen, J.H. Walther, Aeroelastic analysis of bridge sections based on discrete vortex simulations, in: 2nd Int. Symp. on Computational Wind Engineering CWE'96, 1996.
[4] J.C. Wu, Numerical boundary conditions for viscous flow problems, AIAA J. 14 (8) (1976) 1042.
[5] J.C. Wu, U. Gulcat, Separate treatment of attached and detached flow regions in general viscous flows, AIAA J. 19 (1) (1981) 20.
[6] R.B. Kinney, Z.M. Cielak, Analysis of unsteady viscous flow past an airfoil: Part I – theoretical development, AIAA J. 15 (12) (1977) 1712.
[7] J.C. Wu, S. Sampath, N.L. Sankar, A numerical study of unsteady viscous flows around airfoils, AGARD Conf. Proc. vol. 227, Ottawa, Canada, 1977, pp. 24-1-24-18.
[8] M.E. Tasim, R.B. Kinney, Analysis of two-dimensional viscous flow over cylinders in unsteady motion, AIAA J. 22 (5) (1984) 586.
[9] I.H. Tuncer, J.C. Wu, C.M. Wang, Theoretical and numerical studies of oscillating airfoils, AIAA J. 28 (9) (1990) 1615.
[10] J. Carrier, L. Greengard, V. Rokhlin, A fast adaptive multipole algorithm for particle simulations, SIAM J. Sci. Statist. Comput. 9 (4) (1988) 669.
[11] J.H. Walther, Discrete Vortex Method for Two-dimensional Flow past Bodies of Arbitrary Shape Undergoing Prescribed Rotary and Translational Motion. Ph.D. Thesis, Department of Fluid Mechanics, Technical University of Denmark, September 1994.
[12] P.R. Spalart, Vortex methods for separated flows, NASA TM, NASA, June 1988.
[13] J.C. Wu, A theory for aerodynamic forces and moments, Technical Report, Georgia Institute of Technology, September 1978.
[14] E. Simiu, R.H. Scanlan, Wind Effects On Structures, 2nd ed., Wiley, New York, 1986.